Enceladus auroral hiss observations: Implications for electron beam locations

J. S. Leisner,[1] G. B. Hospodarsky,[1] and D. A. Gurnett[1]

Received 15 August 2012; revised 8 October 2012; accepted 6 November 2012; published 17 January 2013.

[1] The Cassini spacecraft has made 20 close flybys of the icy moon Enceladus between its arrival at Saturn in 2004 and 2012. Of those 20, strong whistler mode emissions (often called auroral hiss) were clearly observed on seven encounters. The propagation paths of these emissions are determined by the background magnetic field, which allows their source regions to be studied using simple ray-tracing codes. In this paper, we trace the auroral hiss observations from Cassini's trajectories to possible source locations near Enceladus. We find that all of the detected emissions could be generated by field-aligned electron beams in one of two regions around the moon: upstream of the Saturnward terminator and downstream of the anti-Saturnward terminator. These results suggest that electron beam acceleration near the solid body is a quasi-time-stationary feature of the plasma interaction and that the auroral hiss generated by these beams may be used to remotely study plasma processes in regions separated from the spacecraft.

Citation: Leisner, J. S., G. B. Hospodarsky, and D. A. Gurnett (2013), Enceladus auroral hiss observations: Implications for electron beam locations, *J. Geophys. Res. Space Physics*, *118*, 160–166, doi:10.1029/2012JA018213.

1. Introduction

[2] On the scale of the Saturnian system, the icy moon Enceladus is a point source of the neutrals and dust that are dominant influences on the magnetospheric processes [*Gombosi et al*., 2009]. On a smaller scale, however, the region around Enceladus is a complex interaction between the solid moon, an absorbing body; the neutrals ejected from the moon's south pole [*Dougherty et al*., 2006; *Hansen et al*., 2006; *Porco et al*., 2006]; the dust that also originates at the south pole, but follows different trajectories [*Spahn et al*., 2006; *Kempf et al*., 2008]; and a plasma flow that is time-variable from the perspective of the moon [*Gurnett et al*., 2007]. This interaction has been studied using the observed perturbations in the magnetic field [*Khurana et al*., 2007; *Jia et al*., 2010a; *Jia et al*., 2011] and the ions [*Tokar et al*., 2009], as well as with theory that included the contribution of the plume-derived dust [*Simon et al*., 2011] and simulations to put observations along the spacecraft trajectories into the context of the larger interaction [*Jia et al*., 2010b, 2010c; *Kriegel et al*., 2011].

[3] The effects examined in the above studies have been observed by the Cassini spacecraft since the first close ($<$12 Enceladus radii; 1 R_E = 252 km) flyby of Enceladus in 2005. It was not until later flybys, however, that another feature of this interaction was observed. When Cassini passed through the plume beneath Enceladus' south pole, the radio and plasma wave (RPWS) instrument [*Gurnett et al*., 2004b] detected whistler mode waves that, in a time-frequency spectrogram, formed a sharp-edged funnel shape [*Gurnett et al*., 2011]. The funnel shape spectrum is very similar to the spectrum of auroral hiss emissions observed over Earth's auroral regions [*Gurnett*, 1966] which are produced by quasi-electrostatic whistler mode waves propagating at wave normal angles near the resonance cone [*Mosier and Gurnett*, 1969; *James*, 1976]. The resonance cone is an angle of propagation, measured from the magnetic field direction, which is fixed for a specific frequency but increases monotonically with wave frequency. These waves grow via Landau resonance with an electron beam and are typically generated in a region of particle acceleration parallel to the magnetic field. For a more complete explanation of this growth mechanism and wave characteristics, we refer readers to *Farrell et al*. [1988] and references therein.

[4] The fact that the resonance cone angle can be easily calculated allows the source region to be found by performing ray tracing on these waves through a smoothly varying magnetic field [*Xin et al*., 2006]. *Gurnett et al*. [2011] took advantage of this to perform 2-D ray tracing on the waves observed during Cassini's 21 November 2009 flyby of Enceladus. By propagating waves from different possible source locations, they found two points that were able to match the sharp low-frequency edge of both sides of the observed funnel. They concluded that there were narrow regions of electron beam acceleration between those two points, although located much closer to the moon than the spacecraft. Coincident electron observations with the Cassini Plasma Spectrometer [*Young et al*., 2004] showed magnetic-field-aligned electron beams (pitch angles less than 20°) near the field lines where ray tracing located the sources.

[1]Department of Physics and Astronomy, University of Iowa, Iowa City, Iowa, USA.

Corresponding author: J. S. Leisner, Department of Physics and Astronomy, University of Iowa, Iowa City, IA 52242, USA. (jared-leisner@uiowa.edu)

2169-9380/13/2012JA018213

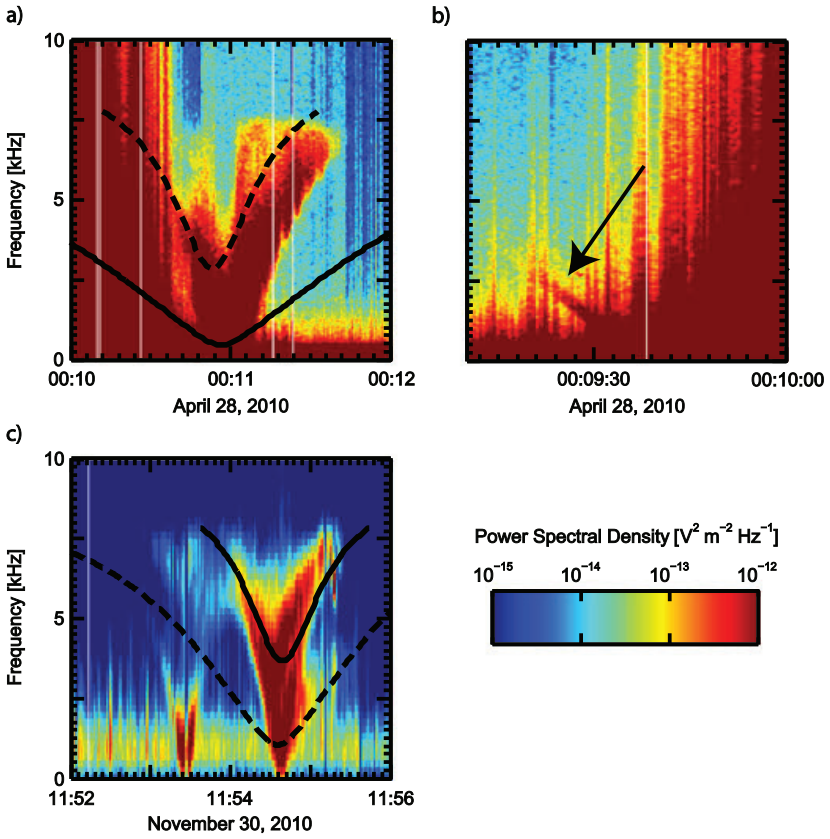

Figure 1. Plasma wave observations made (a and b) south and (c) north of Enceladus with over plotted funnel traces. The dashed lines on Figures 1a and 1c show hypothetical funnels produced by a northward-moving beam and the solid lines show those produced by a southward-moving beam. On Figure 1b, the black arrow points to the funnel partially obscured by dust impacts.

[5] In this paper, we present the results of three-dimensional ray tracing using all of the Cassini flybys with clear resonance cone emissions. Combining the source locations derived from all of the observations, we discuss possible time-stationary source locations around the moon and their implications for particle acceleration in the Enceladus interaction region.

2. Observations

[6] To date, the Cassini spacecraft has made 20 close flybys of Enceladus. During these flybys, the RPWS instrument obtained high-resolution wideband receiver (WBR) data in either the 10 kHz or the 80 kHz filter mode using one antenna (see *Gurnett et al*. [2004b] for a description of the RPWS WBR receivers). A WBR waveform was typically obtained every eighth of a second. A fast Fourier transform is performed on the waveform after it is transmitted to the ground, resulting in a time-frequency spectrogram as shown in Figure 1.

[7] Unfortunately, at Enceladus, there is a strong noise signal due to dust impacts when the spacecraft is near the moon's plume. These impacts on the spacecraft manifest themselves in the RPWS wideband waveforms as voltage spikes with long relaxation times [*Gurnett et al*., 2004a; *Kurth et al*., 2007]. These impacts affect our observations in three ways: (1) Frequent large amplitude voltage spikes cause the receiver gain to decrease, which makes it more difficult to detect weaker real signals present in the time series. (2) The receiver is "dead" to real signals during a dust impact's relaxation time; this is about 1% of the total time series for the 10 kHz receiver and about 10% for the 80 kHz receiver. (3) When the time series is Fourier analyzed, the spikes manifest as a strong broadband signal that can mask and obscure the funnels.

[8] Of the 20 Enceladus flybys through 2012, RPWS has observed clear auroral hiss funnels on the seven flybys shown in Figure 2 (five flybys in the south and two in the north, listed in Table 1). The funnels were all centered on times when Cassini was near the edge of the Enceladus flux tube. The low observation count is understandable since these emissions are guided by the magnetic field and propagate roughly within a 50° cone centered on their source field line. Using the *Gurnett et al*. [2011] source locations, the near-equatorial encounter trajectories early in the mission and in 2011/2012 took Cassini through regions where the waves could not reach or through regions where dust impacts dominate. On the 2008 flybys, the high spacecraft speed caused strong dust-driven noise to appear over a larger region. The 2008 trajectories were also highly inclined, which would change the emission's shape in the spectrogram from a funnel to something not readily recognized.

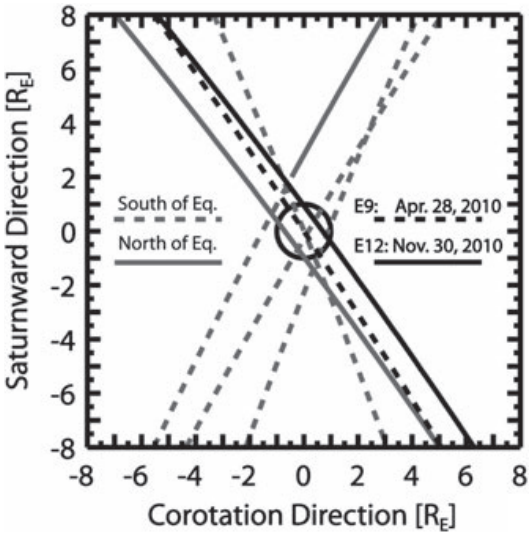

Figure 2. Cassini flybys with funnel observations. The dashed lines are when Cassini was below Enceladus' equatorial plane, and solid lines are when Cassini was above Enceladus' equatorial plane. The dark trajectories are for the flybys used in Figure 1.

[9] Figure 1a shows a funnel observed as Cassini passed south of Enceladus' anti-Saturnward limb (E9: 28 April 2010). The saturated broadband power present until 00:10:35 is due to impacts from plume dust particles. The funnel extends up to about 7.5 kHz and has a well-defined right-hand branch. Part of the left-hand branch can be observed outside of the dust-dominated region, but the lower edge of that funnel is completely lost above 3 kHz. This overlap with the noise from the dust impacts reduces our ability to use ray tracing to precisely locate the source region. When Cassini is closer to Enceladus' south pole, there are sometimes small funnels partially obscured by the dust impacts (Figure 1b). These funnels do not reach the higher frequencies that the larger funnels do, but we analyze them when possible.

[10] In the northern hemisphere (Figure 1c), the dust density is low enough that impacts do not cause much difficulty with observing the auroral hiss. On this flyby (E12: 30 November 2010), three sets of funnels were observed. The first (11:53:27) is strong up until ~3 kHz and fades out by ~5 kHz. The second funnel (11:53:45) is much weaker and is only present at higher frequencies. This "lack" of lower frequencies is due to Cassini not crossing field lines where the lower frequencies could propagate to the spacecraft. The final set of funnels (11:54:35) is not a single emission, but rather multiple funnels that are stacked on top of one another in the spectrogram.

3. Analysis

3.1. Auroral Hiss Propagation

[11] Auroral hiss propagates at an angle to the magnetic field known as the resonance cone angle. This angle (ψ) is a function of wave frequency (f), the local electron plasma frequency (f_p), and the local electron cyclotron frequency (f_c) [*Gurnett et al*., 1983; *James*, 1976].

$$\tan^2\psi = f^2 f_p^2 \left(f_p^2 - f^2\right)^{-1} \left(f_c^2 - f^2\right)^{-1} \quad (1)$$

[12] At Enceladus, the plasma frequency is usually above 60 kHz [*Gurnett et al*., 2007, 2011] and the typical 325 nT magnetic field [*Dougherty et al*., 2006] yields an electron cyclotron frequency of ~9 kHz. From equation 1, it is clear that the auroral hiss at Enceladus must then be below 9 kHz and will be much smaller than the plasma frequency. For that situation, *Xin et al*. [2006] showed that the resonance cone angle is given by

$$\sin\psi = f f_c^{-1} \quad (2)$$

[13] Our analysis uses a simple dipole magnetic field that is displaced 0.037 R_S north of the equatorial plane [*Dougherty et al*., 2004] and has a 325 nT field at the moon. The bend and enhancement in the magnetic field due to Enceladus' plume [*Khurana et al*., 2007; *Jia et al*., 2010a, 2011] are neglected. The observed field bend is less than 5° and the enhancement is up to about 10%. From equation 2, it is clear that these variations in the magnetic field would affect the higher frequencies most, but those waves propagate at large angles to the field and would not be within the disturbed region for long.

3.2. Ray Tracing

[14] We traced by hand the upper and lower frequency edges of each funnel observed during Cassini's Enceladus flybys. At each step along Cassini's trajectory, we propagate waves at these two frequencies at angles from the magnetic field calculated using equation 2, for all azimuths around the magnetic field, and both parallel and anti-parallel to the magnetic field. These ray paths form cones of finite thickness that define the regions in which any possible sources must lie. When combining observations (for a single funnel)

Table 1. Enceladus Auroral Hiss Observations

Flyby	Date	Hemisphere	Funnel Center Time[a]	Source Center Location[b]
E2	14 July 2005	South	19:52:05	1.86, 3.22
E7	2 November 2009	South	07:42:45	0.22, −0.46
			07:42:57	0.54, −1.26
E8	21 November 2009	South	02:09:50	0.65, 0.24
		South	02:11:38	1.34, 1.44
E9	28 April 2010	South	00:09:22	0.46, −0.65
		South	00:10:58	−0.55, 0.89
E11	13 August 2010	South	22:28:35	0.22, 1.16
			22:32:15	1.06, 1.91
E12	30 November 2010	North	11:53:26	−0.03, 0.96
			11:54:27	0.90, −0.26
			11:54:36	0.97, −0.43
			11:54:45	1.24, −0.83
E13	21 December 2010	North	01:07:58	−0.79, 0.07
			01:09:13	0.15, −1.22

[a]Average time of the center-most points observed for the funnels. If a funnel only has one side, the centermost point for that funnel is given.
[b]Center of possible source region projected onto equatorial plane calculated by taking the average X and average Y positions and given in moon radii in Enceladus interaction coordinate system.

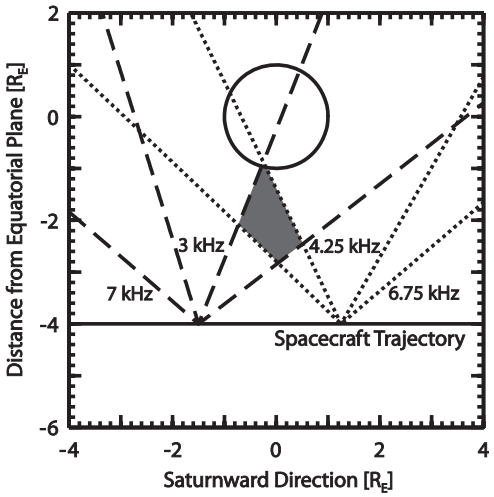

Figure 3. Cartoon example of finding the possible source region. Upper and lower frequencies are traced moonward from two observation points on a hypothetical trajectory.

along the entire trajectory, the source must lie within the intersection of all of these cones. We save that region of overlap as the source for the auroral hiss funnel analyzed.

[15] Figure 3 shows a simplified two-dimensional cartoon of this process. We used an arbitrary spacecraft trajectory where the funnel was traced at two points. The dashed and dotted lines show the ray paths for the two spacecraft locations (for simplicity, we show only the ray paths that yield sources near the moon). Each observation, on its own, defines a large space where the sources could contribute to the funnel. When the two are combined, however, the source region is restricted to a small area beneath the moon (shaded grey). In the three-dimensional picture, the source region extends into and out of the page to form something like a bowtie shape in the *XY* plane.

[16] As discussed by *Xin et al*. [2006], each source region is non-unique. In our cartoon, there could also be a source of northward-propagating auroral hiss $6\,R_E$ below the moon. Unless a trajectory takes the spacecraft from north of to south of the source region, it is not possible to use the RPWS wideband receiver to discriminate between northward and southward propagating waves for a single funnel observation. To determine this, it is necessary to combine observations from both above and below Enceladus. Two convenient flybys to test this are E9, when Cassini passed to the south of Enceladus, and E12, when it passed to the north. The flybys' strongest funnels both had valid sources along the $[X,Y] = [0.7, -0.7]\ R_E$ axis. (This axis is defined in the Enceladus interaction coordinate system (ENIS) where *X* is in the ideal corotation direction, *Y* is positive toward Saturn, and *Z* is northward.)

[17] For these funnels, the source degeneracy led our ray tracing to consider $[0.7, -0.7, -2]\ R_E$ and $[0.7, -0.7, 2]\ R_E$ valid sources for the E9 and E12 funnels, respectively. In Figure 1, we propagate waves from those two possible sources to each of the spacecraft trajectories. The dashed line in Figure 1a shows that the (northward-propagating) waves for the first source fit within the E9 funnel. The solid line, however, shows that the second source's (southward-propagating) waves are incompatible with the observations at frequencies above ~1 kHz, since there are no waves observed. Figure 1b shows the reverse: the second source is compatible with the observations but the first source is not. We do not show them in this paper, but we have repeated this exercise for all of the flybys with the same result: only the waves that propagate away from Enceladus are consistent with all of the observations. In our subsequent analysis, we only consider those sources to be valid possibilities.

3.3. Source Locations in the *XY* Plane

[18] At Enceladus, the magnetic field is predominantly vertical (in the *Z* direction). Since the magnetic field orders the Enceladus interaction, it is convenient to collapse all possible source locations into the *XY* plane. In this view, if a location is marked, then the real potential source location is (roughly speaking) somewhere on the magnetic field line that passes through that *XY* location in Enceladus' equatorial plane. In this section, we will refer to an area or region being a potential source as a shorthand method of referring to the three-dimensional space of potential sources.

[19] Figure 4 shows the number of funnels that potentially arise from each location (projected onto the *XY* plane) for southward beams (Figure 4a), northward beams (Figure 4b), and all beams (Figure 4c). The darker an area's color, the higher the number of funnels that could have been generated in that region. Following the discussion in section 3.2, this figure was generated using sources within the vertical range $[-1.4, 1]\ R_E$ for both northward and southward funnels.

[20] The size of each individual funnel's region is related to Cassini's distance from the source and the quality of the funnel tracing. When the spacecraft is farther from the source, such as for the *Gurnett et al*. [2011] analysis, the funnel is larger in spatial extent. When tracing the edges of a single funnel back in toward the distant source, a large volume of space is capable of producing emissions consistent with the observations. When both sides of the funnel are present at all frequencies, this is not a problem. During actual observations, however, that condition is not always fulfilled. When Cassini is south of Enceladus, the numerous dust impacts appear in the RPWS spectrograms as broadband power (left side of Figure 1a). This pseudo-power obfuscates the funnels and artificially shortens the length of the trace, which results in a larger-than-expected source region. This visibility issue is worst near the plume, but is still present more than $7\,R_E$ south of the moon [see *Gurnett et al*., 2011, Figure 3].

[21] The smallest, and thus most certain, southward source regions (Figure 1a) are near the edges of the moon. On the anti-Saturnward side are two whose area of intersection is completely overlapped by a third, slightly larger source region. The larger region partially intersecting that common area covers both sides of the Enceladus flux tube, which renders it useless in terms of determining the side of the moon that the source is located. On the Saturnward side of Enceladus, there is a small source region slightly upstream of the flow terminator. The terminator side of that region is also consistent with three of the larger sources. All three imprecisely sourced funnels may have been that part of Enceladus' Saturnward side, but it is not possible to determine that with any certainty.

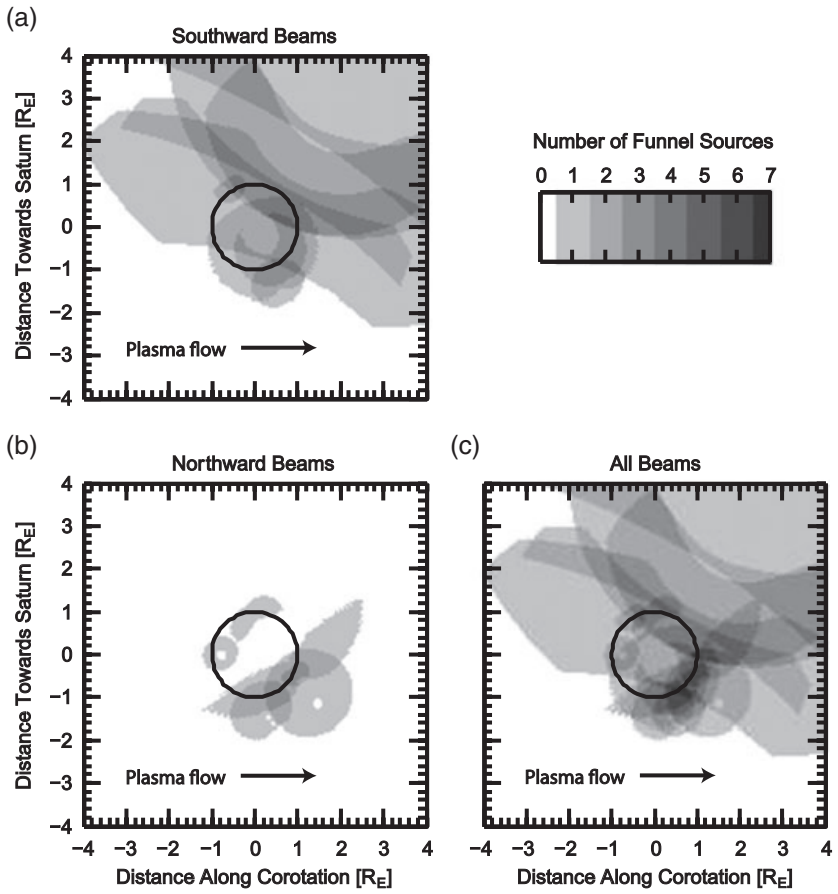

Figure 4. Distribution of possible funnel source beam locations projected onto the equatorial plane. Included are all possible sources within $Z = [-1.4, 1.0]$ R_E. The color gives the number of funnel sources per location and Figure 4 shows (a) just southward sources, (b) just northward sources, and (c) all sources.

[22] Due to the decreased dust density and Cassini's close flybys in the northern hemisphere, the northward beams locations (Figure 4b) tend to be smaller. As in the other hemisphere, there is a cluster downstream of the anti-Saturnward flow terminator. In this instance, however, the grouped sources were from funnels observed on only two flybys. There are two additional sources on the opposite side of the moon, but there is no spatial overlap between them.

[23] When the northward and southward beams are considered together (Figure 4c), there is significant overlap between the anti-Saturnward sources and little overlap between the Saturnward sources. Of the 16 funnels observed over all of the flybys, seven could originate downstream of the anti-Saturnward terminator.

4. Discussion

[24] When considering auroral hiss at Enceladus, it is convenient to first consider which electrons are not generating these emissions. *Pryor et al*. [2011] found a field-aligned distribution during a 2008 moon flyby, between ~5 and 15 R_E downstream of the moon's anti-Saturnward flank and at energies of ~1 keV. When the spacecraft got closer to the moon's flow terminator, to where we trace the funnel sources, the beam disappeared. While this beam could generate the Enceladus auroral footprint, as concluded by *Pryor et al*., it does not extend to the auroral hiss source regions that we find and no such emissions were observed on or near those field lines.

[25] In the simple mass-loaded plasma cartoon [*Kivelson*, 2004], field-aligned currents close the cross-field currents in the planet's ionosphere and the mass-loading region. In Saturn's southward magnetic field, these currents are antiplanetward on the Saturnward side of Enceladus and planetward on the other. If parallel electric fields were accelerating electrons to provide the necessary current due to the mass loading alone, there are differences between what would be expected and what is observed.

[26] The first expectation would be that the funnel sources would be ordered by the mass-loading region, Enceladus' plume, not by the moon itself. As illustrated in Figure 1 and discussed in section 3.2, the observations are only consistent with sources at the solid body. Sources away from the moon would have produced funnels significantly different than those observed. The second expectation would be that, on one side of the mass-loading center, there would only be a single funnel propagating toward the spacecraft. The auroral hiss observation at Io [*Xin et al*., 2006] is consistent with this picture; when Galileo passed south of Io, there was only one funnel and it was observed on the side with the northward current. During Cassini flybys of Enceladus, northward and southward funnels were observed on both

flanks of the moon. Additionally, the emissions originate from near Enceladus itself and not from the mass-loading center.

[27] The field-aligned currents are different in an Enceladus-like interaction, however. When a solid, non-conducting body is displaced (along the magnetic field) from the mass-loading center, a hemisphere coupling current system arises at the edge of the body's flux tube [*Saur et al*., 2007; *Simon et al*., 2011]. The current distribution is similar about the solid body, so the previous discussion holds, but there is a second current system on the strongly mass-loading side (below) of the solid body [illustrated in *Simon et al*. 2011, Figure 5].

[28] South of Enceladus, the plume (modeled as a cylinder in the *Simon et al*. cartoon) requires the same field-aligned current as in the simple interaction: a moonward current on the Saturnward side and an anti-moonward on the other. Because the plume's core is narrower (in the cross-flow direction) than Enceladus, closing currents flow inside of the moon's flanks. These currents, as expected, are in the opposite direction of the plume-specific currents: anti-moonward on the Saturnward side and moonward on the other. If these currents require the acceleration of electrons, then there could be southward beams on both sides of the moon.

[29] There are, however, two issues with using just this picture as the generation mechanism for the funnels: (1) there would still be only one northward beam in the northern hemisphere and (2) the southern hemisphere's southward beam on the Saturn side would be inside of the moon's flux tube and not on the edge.

[30] For the first issue, the northern hemisphere could be an additional mass-loading source that, like the plume, is narrower than the moon. However, no evidence has been presented yet for any such neutral population. Additionally, that hypothetical population would encounter issue 2. The ray-tracing results show that the beams would be at and outside of the Enceladus flux tube, not inside of it.

[31] For the southern hemisphere, the magnetometer data show that there are field-aligned currents, caused by a probable combination of plasma and dust effects, outside of the Enceladus flux tube. *Jia et al*. [2011] and *Simon et al*. [2011] show strong rotations in the magnetic field out to about $-1.3\,R_E$ on the anti-Saturnward side of Enceladus and at the Saturnward edge of the moon. The beams that *Gurnett et al*. [2011] observed with the E8 auroral hiss funnels also coincided with transverse magnetic perturbation similar to those near the moon. Although there have not been direct observations of beams along Enceladus' flanks, it is not unreasonable to suspect that the *Gurnett et al*. observations map to the perturbations reported in the magnetometer data.

5. Conclusions

[32] Auroral hiss funnels have been present on all non-high-inclination flybys through the Enceladus flux tube. Using a ray-tracing code, we find that these funnels map to two regions near the moon: the quadrant upstream of the Saturnward flow terminator and the quadrant downstream of the anti-Saturnward flow terminator. Sources in both of these regions for both the northward and the southward funnels are consistently observed, which suggests that electron beam generation is a steady state feature of the moon-plasma interaction. These areas near Enceladus contain strong field-aligned currents that may be responsible for all of the beams. An electron beam has been observed for only the anti-Saturnward source of southward-propagating funnels, so we cannot rule out other acceleration mechanisms, such as surface charging. For the northern hemisphere, a small mass-loading region may also contribute to the current system and electron acceleration. Continued monitoring of these funnels may provide an additional diagnostic tool for studying the Enceladus interaction region on future flybys.

[33] **Acknowledgment.** This research has been funded by NASA through contract 1415150 with the Jet Propulsion Laboratory.

References

Dougherty, M. K., et al. (2004), The Cassini magnetic field investigation, *Sp. Sci. Rev.*, *114*, 331–383, doi:10.1007/s11214-004-1432-2.

Dougherty, M. K., K. K. Khurana, F. M. Neubauer, C. T. Russell, J. Saur, J. S. Leisner, and M. E. Burton (2006), Identification of a dynamic atmosphere at Enceladus with the Cassini magnetometer, *Science*, *311*, 1406–1409, doi:10.1126/science.1120985.

Farrell, W. M., D. A. Gurnett, P. M. Banks, R. I. Bush, and W. J Raitt (1988), An analysis of whistler mode radiation from the Spacelab 2 electron beam, *J. Geophys. Res.*, *93*(A1), 153–161.

Gombosi, T. I., T. P. Armstrong, C. S. Abridge, K. K. Khurana, S. M. Krimigis, N. Krupp, A. M. Persoon, and M. F. Thomsen (2009), Saturn magnetospheric configuration, in Saturn from Cassini-Huygens, edited by M. K. Dougherty, L. W. Esposito, and S. M. Krimigis, Springer, London.

Gurnett, D. A. (1966), A satellite study of VLF hiss, *J. Geophys. Res.*, *71*, 5599–5615.

Gurnett, D. A., et al. (2011), Auroral hiss, electron beams and standing Alfvén wave currents near Saturn's moon Enceladus, *Geophys. Res. Lett.*, *38*, L06102, doi:10.1029/2011GL046854.

Gurnett, D. A., et al. (2004a), Radio and plasma wave observations at Saturn from Cassini's approach and first orbit, *Science*, *307*, 1255–1259, doi:10.1126/science.1105356.

Gurnett, D. A., et al. (2004b), The Cassini radio and plasma wave investigation, *Sp. Sci. Rev.*, *114*, 395–463, doi:10.1007/s11214-004-1434-0.

Gurnett, D. A., A. M. Persoon, W. S. Kurth, J. B. Groene, T. F. Averkamp, M. K. Dougherty, and D. J. Southwood (2007), The variable rotation period of the inner region of Saturn's plasma disk, *Science*, *316*, 442–445, doi:10.1126/science.1138562.

Gurnett, D. A., S. D. Shawhan, and R. R. Shaw (1983), Auroral hiss, z mode radio, and auroral kilometric radiation in the polar magnetosphere: DE 1 observations, *J. Geophys. Res.*, *88*, 329–340, doi:10.1029/JA088iA01p00329.

Hansen, C. J., L. Esposito, A. I. F. Stewart, J. Colwell, A. Hendrix, W. Pryor, D. Shemansky, and R. West (2006), Enceladus' water vapor plume, *Science*, *311*, 1422–1425, doi:10.1126/science.1121254.

James, H. G. (1976), VLF Saucers, *J. Geophys. Res.*, *81*(4), 501–514, doi:10.1029/JA081i004p00501.

Jia, Y. D., C. T. Russell, K. K. Khurana, J. S. Leisner, Y. J. Ma, and M. K. Dougherty (2010a), Time-varying magnetic field environment near Enceladus as seen by the Cassini magnetometer, *Geophys. Res. Lett.*, *37*, L09203, doi:10.1029/2010GL042948.

Jia, Y.-D., C. T. Russell, K. K. Khurana, Y. J. Ma, W. Kurth, and T. I. Gombosi (2010b), Interaction of Saturn's magnetosphere and its moons: 3. Time variation of the Enceladus plume, *J. Geophys. Res.*, *115*, A12243, doi:10.1029/2010JA015534.

Jia, Y.-D., C. T. Russell, K. K. Khorana, Y. J. Ma, D. Najib, and T. I. Gombosi (2010c), Interaction of Saturn's magnetosphere and its moons: 2. Shape of the Enceladus plume, *J. Geophys. Res.*, *115*, A04215, doi:10.1029/2009JA014873.

Jia, Y. D., C. T. Russell, K. K. Khurana, H. Y. Wei, Y. J. Ma, J. S. Leisner, A. M. Persoon, and M. K. Dougherty (2011), Cassini magnetometer observations over the Enceladus poles, *Geophys. Res. Lett.*, *38*, L19109, doi:10.1029/2011GL049013.

Kempf, S., U. Beckmann, G. Moragas-Klostermeyer, F. Postberg, R. Srama, T. Economou, J. Schmidt, F. Sphan, and E. Grün, (2008), The E-ring in the vicinity of Enceladus I. Spatial distribution and properties of the ring particles, *Icarus*, *193*, 420.

Khurana, K. K., M. K. Dougherty, C. T. Russell, and J. S. Leisner (2007), Mass loading of Saturn's magnetosphere near Enceladus, *J. Geophys. Res.*, *112*, A08203, doi:10.1029/2006JA012110.

Kivelson, M. G. (2004), Moon-magnetosphere interactions: A tutorial, *Adv. Sp. Res.*, *33*, 2061–2077, doi:10.1016/j.asr.2003.08.042.

Kriegel, H., S. Simon, U. Motschmann, J. Saur, F. M. Neubauer, A. M. Persoon, M. K. Dougherty, and D. A. Gurnett (2011), Influence of negatively charged plume grains on the structure of Enceladus' Alfvén wings: Hybrid simulations versus Cassini Magnetometer data, *J. Geophys. Res.*, *116*, A10223, doi:10.1029/2011JA016842.

Kurth, W. S., T. F. Averkamp, D. A. Gurnett, and Z. Wang (2007), Cassini RPWS observations of dust in Saturn's E ring, *Plan. Sp. Sci.*, *54*, 988–998, doi:10.1016/j.pss.2006.05.011.

Mosier, S. R., and D. A. Gurnett (1969), VLF measurements of the Poynting flux along the geomagnetic field with the Injun 5 satellite, *J. Geophys. Res.*, *74*, 5675–5687, doi:10.1029/JA074i024p05675.

Porco, C. C., et al. (2006), Cassini observes the active south pole of Enceladus, *Science*, *311*, 1393–1401, doi:10.1126/science.1123013.

Pryor, W. R., et al. (2011), The auroral footprint of Enceladus on Saturn, *Nature*, *472*, 331–333, doi:10.1038/nature09928.

Saur, J., F. M. Neubauer, and N. Schilling (2007), Hemisphere coupling in Enceladus' asymmetric plasma interaction, *J. Geophys. Res.*, *112*, A11209, doi:10.1029/2007JA012479.

Simon, S., J. Saur, H. Kriegel, F. M. Neubauer, U. Motschmann, and M. K. Dougherty (2011), Influence of negatively charged plume grains and hemisphere coupling currents on the structure of Enceladus' Alfvén wings: Analytical modeling of Cassini magnetometer observations, *J. Geophys. Res.*, *116*, A04221, doi:10.1029/2010JA016338.

Spahn, F., et al. (2006), Cassini dust measurements at Enceladus and implications for the origin of the E ring, *Science*, *311*, 1416–1418, doi:10.1126/science.1121375.

Tokar, R. L., R. E. Johnson, M. F. Thomsen, R. J. Wilson, D. T. Young, F. J. Crary, A. J. Coates, G. H. Jones, and C. S. Paty (2009), Cassini detection of Enceladus' cold water-group plume ionosphere, *Geophys. Res. Lett.*, *36*, L13203, doi:10.1029/2009GL038923.

Young, D. T., et al. (2004), Cassini plasma spectrometer investigation, *Sp. Sci. Rev.*, *114*, 1–112, doi:10.1007/s11214-004-1406-4.

Xin, L., D. A. Gurnett, and M. G. Kivelson (2006), Whistler mode auroral hiss emissions observed near Jupiter's moon Io, *J. Geophys. Res.*, *111*, A04212, doi:10.1029/2005JA011411.